MIPR to AROFE AOARD contract # 044008

Final Report to AROFE on the Proposed Work

High resolution real time phase contrast radiology study of hydrodynamic in micrometer scale

Principal Investigators: M. K. Wu, Y. K. Hwu and C. D. Chen
Research Assistant: W.H. Chao
Institute of Physics, Academia Sinica, Taipei, Taiwan

Abstract

This report describes in detail our experimental observations of magnetic fluid flow in microscopic channel using high resolution real time phase contrast radiology. Tasks accomplished including the preparation of Fe_3O_4 nano-particles by coprecipitation technique; the fabrication of micro-fluidic channel using lithography technique; and the direct observations of magnetic fluid flow in a micro-tube under the influence of external magnetic fields and various flowing speeds. We conclude that the magnetic nanoparticle fluid behavior can be tuned by setting proper controlled parameters

I. Introduction

This collaborative effort aims at using the newly developed X-ray phase contrast microradiology technique[1—7] to achieve direct imaging of fluid hydrodynamics in microfluidic devices. At the initial phase of the studies, our work will concentrate in using the technique to investigate the internal dynamics of the formation of the bubbles in a microfluidic device. With such information, one can tie the images of the internal bubble formation with the external formation of the sprays to support the numerical simulation, which provides valuable information to improve the functionality of ink-jet printer head.

The second part of this proposed work will study the mechanism of nano-particle flow in micro-scaled fluidic channels. It has been shown that colloids can be directly manipulated through the application of external fields. The processes of electrophoresis, dielectrophoresis, and magnetophoresis have all been used to control and influence the motion of small particles in solution. This noncontact, noninvasive technique eliminates the need to physically interface to the macroscopic world and allows for the manipulation of complex objects or multiple objects at once, as would be required for the actuation of a microfluidic valve or pump. In this proposal, we expect to start from a particle-based approach to microfluidic flow generation and control; and then provide a powerful technique for the creation of complex, highly integrated, microscale total analysis systems.

II. Experiments

A. Investigation of the dynamics of bubbles in a microfluidic device

First, we have made groove-type PDMS fluidic channels by means of standard

Report Documentation Page

Form Approved
OMB No. 0704-0188

1. REPORT DATE	2. REPORT TYPE	3. DATES COVERED
05 SEP 2006	**Final Report (Technical)**	**06-07-2004 to 06-10-2005**

4. TITLE AND SUBTITLE	5a. CONTRACT NUMBER
High resolution real time phase contrast radiology study of hydrodynamic in micrometer scale	5b. GRANT NUMBER
	5c. PROGRAM ELEMENT NUMBER
6. AUTHOR(S)	5d. PROJECT NUMBER
Maw-Kuen Wu	5e. TASK NUMBER
	5f. WORK UNIT NUMBER
7. PERFORMING ORGANIZATION NAME(S) AND ADDRESS(ES)	8. PERFORMING ORGANIZATION REPORT NUMBER
Academia Sinica,128 Academia Rd.,,Section 2,Nankang, Taipei, Taiwan,TE,11529	**AOARD-044008**
9. SPONSORING/MONITORING AGENCY NAME(S) AND ADDRESS(ES)	10. SPONSOR/MONITOR'S ACRONYM(S)
The US Resarch Labolatory, AOARD/AFOSR, Unit 45002, APO, AP, 96337-5002	**AOARD/AFOSR**
	11. SPONSOR/MONITOR'S REPORT NUMBER(S)

12. DISTRIBUTION/AVAILABILITY STATEMENT

Approved for public release; distribution unlimited

13. SUPPLEMENTARY NOTES

14. ABSTRACT

14. ABSTRACT Investigation of achieving direct imaging of fluid hydrodynamics in the microfluidic devices using a newly developed X-ray phase contrast radiology technique. The capability of direct imaging in real time of this new technique allows us to study the internal dynamics of the formation of the bubbles in respond to the localized heat or vibration in a microfluidic device. With such information, one can tie the images of the internal bubble formation with the external formation of the sprays to support the numerical simulation, which can be used to improve the functionality of ink-jet printer head. Apart from the ink flow study, one can also study mechanism of nano-particle flow in micro-scaled fluidic channels, which may eventually lead to the better understanding of the mechanism of drug delivery.

15. SUBJECT TERMS

Nanotechnology, Fluid Dynamics

16. SECURITY CLASSIFICATION OF:			17. LIMITATION OF ABSTRACT	18. NUMBER OF PAGES	19a. NAME OF RESPONSIBLE PERSON
a. REPORT	b. ABSTRACT	c. THIS PAGE			
unclassified	**unclassified**	**unclassified**		**17**	

photolithography techniques. A type of thick photo-resist, SU8, with the shape of microfluidic channel was used to mold the PDMS into the groove-type fluidic channel shown as figure 1. Then the PDMS with fluidic channel and glass were bonded together where the surface of the PDMS was activated by oxygen plasma. To check the function of the channels, distilled water was injected into one end of the PDMS reservoir through Teflon tubes. Fig.2 shows schematically the set-up with tubes plugged into PDMS bricks with two adapters, one for inlet and the other for outlet. Distilled water passed through the 10-□m-wide channel smoothly without introducing air bubbles as we expected. We can thus proceed to study the mechanism of nano-particle flow, which can be directly manipulated through the application of external fields in this micro-scaled fluidic channel.

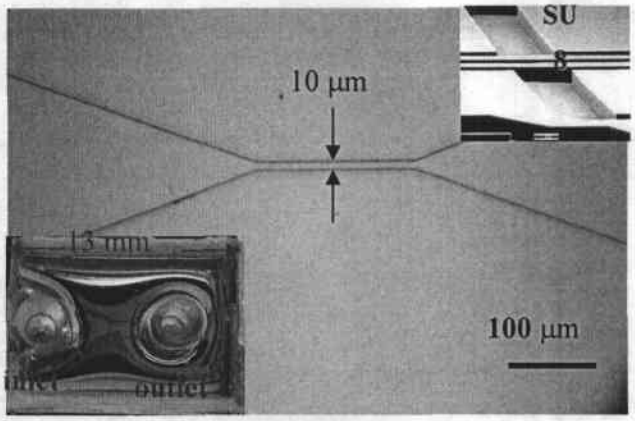

Fig. 1. A 10 μm-wide microfluidic channel made on the bottom side of the PDMS brick. Inset on the lower-left corner: Top view of the PDMS brick. Region marked by the red square is the fluidic channel shown on the main panel. Insert on the upper-right corner: Inverted fluidic channel on the SU8 mold. The scale bar is 100 μm.

In additional to the PDMS fluidic channels, we have also made effort on micro channels made on quartz substrates. This quartz channel was etched by an inductively-coupled-plasma etcher using CF_4 as reacting gas, and with a Cr film as etch mask. The Cr film was made by standard photolithography with a minimum feature size of 8 □m. The depth of the trenches was about 10 □m, which, together with the top mica cover sheet, forms a fluidic channel.

After the success in the fabrication of the device, we immediately examined it with X-ray microscopy to make sure that we can clearly observe the fabricated pattern. Figure 2 shows the microstructures imaged by X-ray microscopy. The high penetration of X-ray together with the phase contrast enhancement successful image the microstructure even with the thick substrate.

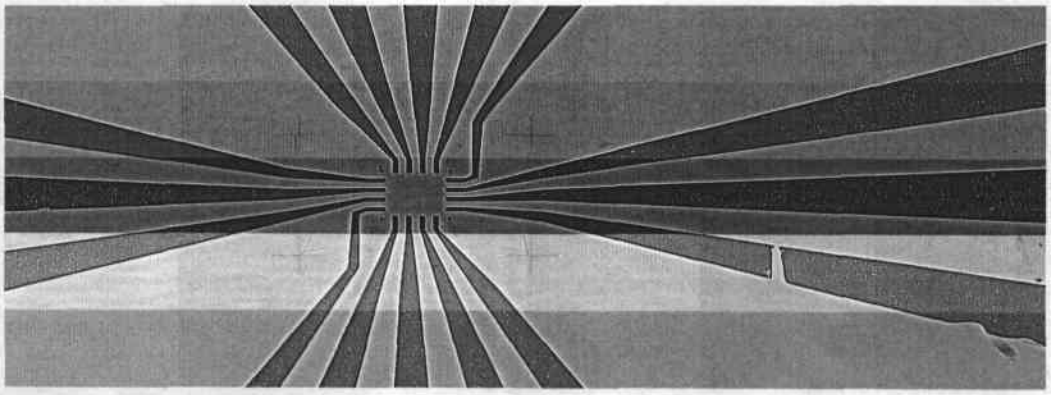

Figure 2. Image of the quartz micro-trenches by X-ray microscopy.

We have also successfully extracted 3D information of the fabricated trenches by rotating the sample with respect to the x-ray beam. However, limited by the slab geometry of the sample, only images taken from +45 to -45 degree rotation with respect to the normal x-ray incidence were captured as shown in Fig. 3.

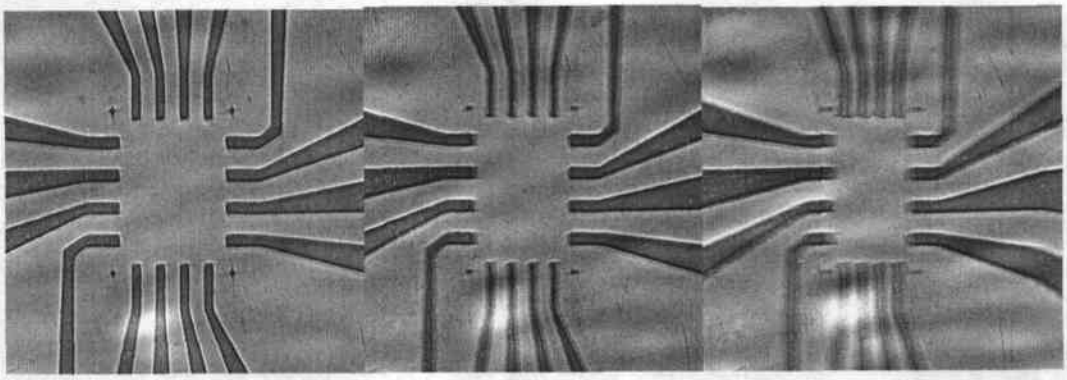

Figure 3. 3D-image of the micro-device fabricated by rotating the sample.

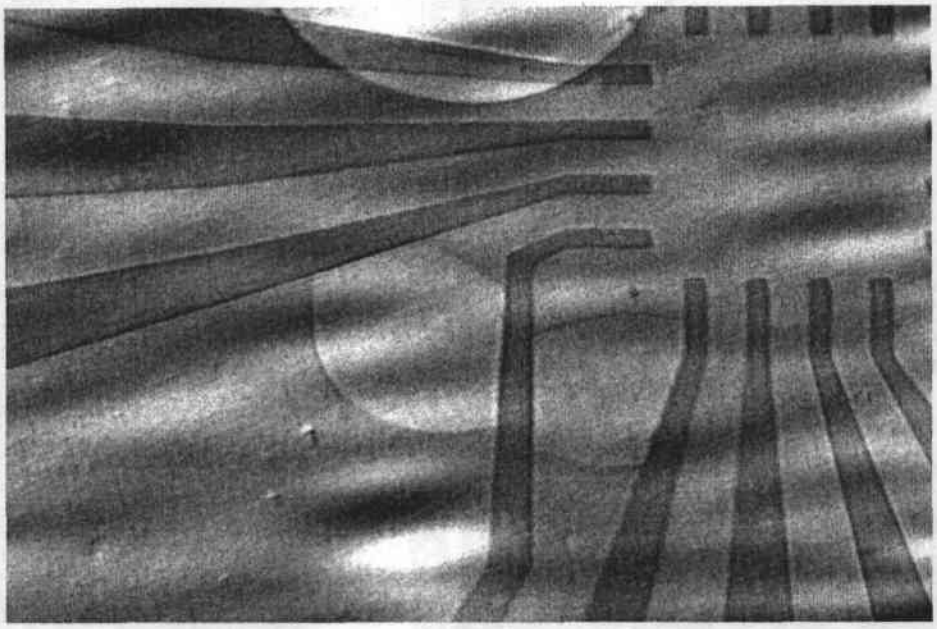

Figure 4: Injection of water droplet to the sample. The water bubbles are clearly observable

To make further test whether the proposed work is achievable, we used water as the testing fluid and inject a small amount into the micro-trenches. Figure 4 shows few snap shots extracted from the time sequence. The absorption contrast is not significant, as we expected, however, the phase effect on the edge, as the edge of the bubble shown in the figure, of the solution allows us to detect the presence of the solution.

The above initial successful demonstration gave us great confidence to proceed the second phase of our proposed experiments to continue with Fe_3O_4 containing fluid and to observe its flow pattern in the micro-fluidic channels.

B. Magnetic microfluid with and without external magnetic fields

The magnetic fluid used in this experiment is prepared by mixing magnetic Fe_3O_4 nanoparticles with DI water. To simplify the preparation of experimental set up, we used Teflon micro-tubes with diameter ranging from 100 μm to 1000 μm to mimic the microfluidic channel. The average size of Fe_3O_4 nanoparticle is about 100 nm, There is no conglomeration of these nanoparticles due to repulsive force arising from the surfactant existing on their surfaces. Figure 5 displays the particle size distribution of the nanoparticle we synthesized, and figure 6 shows their magnetic hysteresis curves. The data clearly demonstrate that these Fe_3O_4 particles are super-paramagnetic with diameter roughly 90-100 nm, and the fluids with higher concentration are more strongly magnetic. The flow of the magnetic fluid was observed using the X-ray microscopy setup at Pohang Synchrotron facility.

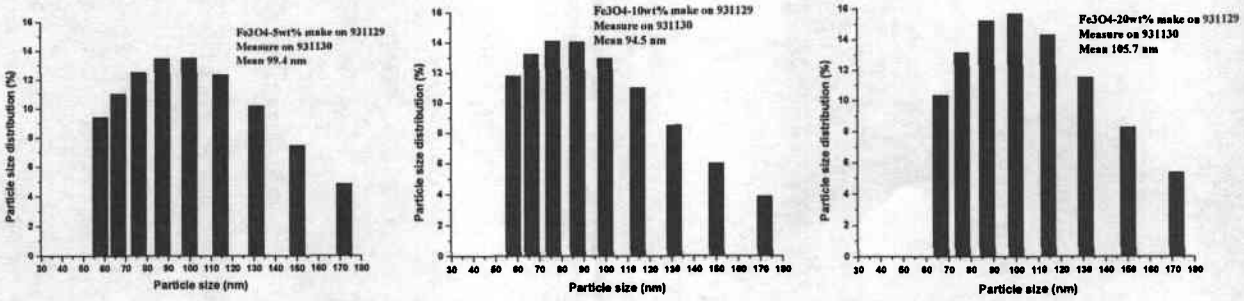

Figure 5. The particle size distributions of Fe_3O_4 with different concentrations; from left are 5wt%, 10 wt% and 20 wt%, respectively.

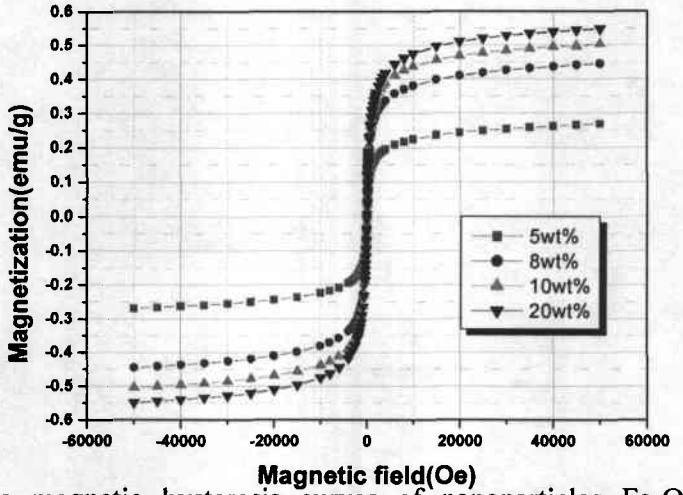

Figure 6. The magnetic hysteresis curves of nanoparticles Fe_3O_4 with different concentrations.

I. Observations of magnet fluid without external magnetic field

The driving force for the flow of magnetic fluid is supplied by a Wriggle pump so that the magnetic fluid flowed in the tube at contact speed. Without the application of any magnetic field, in order to observe the nanoparticles, which were uniformly dispersed in the fluid, we purposely introduced an air-bubble so that we can use the

phase contrast presented at the interfaces between the air-bubble and magnetic fluid to observe the fluid flow. The observed results are shown in Figure 7. We can clearly observe the fluid flow as following the flow of the bubble. This result further support the enhanced contrast with the presence of air bubble as demonstrated in part A.

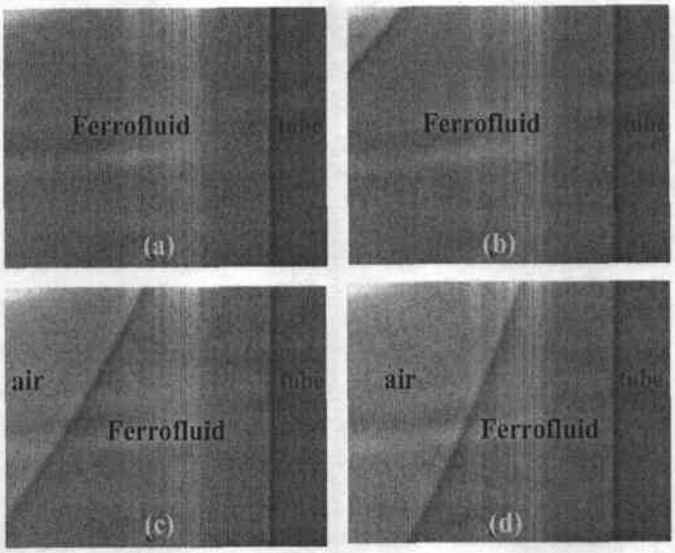

Figure 7: X-ray microscopy image of the magnetic fluid with an artificial bubble to increase the contrast. The white lines are noise during filming; dark regions are where nanoparticles aggregate. The flow behavior is shown in movie 1.

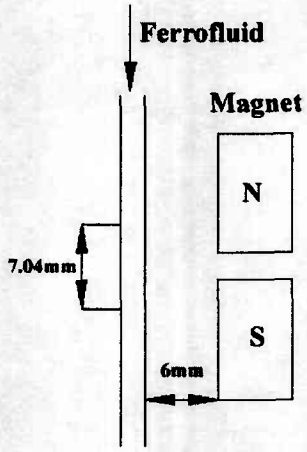

Figure 8: The spatial relation between the microfluid system and magnets.

II. Observations of magnet fluid in a single magnet locates parallel to the tube

We then applied a magnet, which was placed parallel to the outside of the tube, as shown in the schematic diagram (Fig. 8). The magnetic field caused the nanoparticles to aggregate so that we can easily observe the flow of some relatively larger particles along the tube, as shown in figure 9. The observations showed that the magnetic fluid was affected by magnetic field such that the magnetic nanoparticles appear exactly following the magnetic field lines, as evidenced from figures 10 and 11.

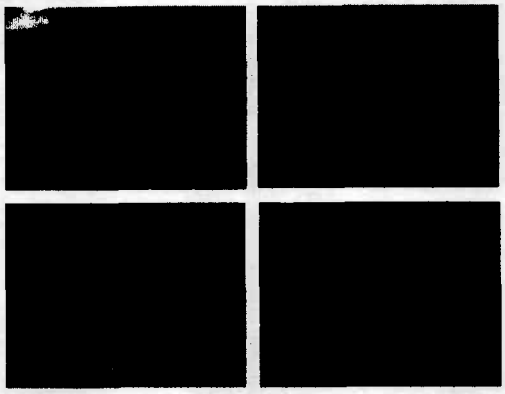

Figure 9: The flow behavior of nanoparticles in magnetic field, we can see clearly the flow of the accumulated particles, as shown in Movie 2.

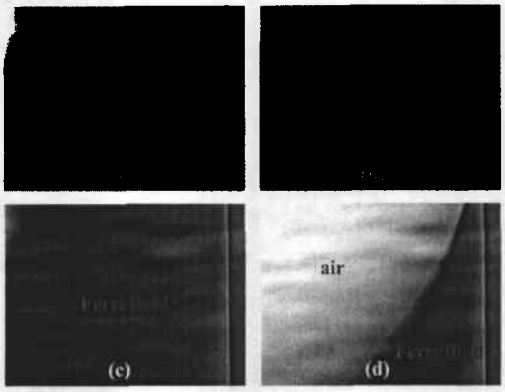

Figure 10. An air bubble was introduced to the microfluid in the presence of magnetic field to enhance phase contrast between the air bubble and nanoparticle. The darker region is where nanoparticles aggregate by magnetic field. The flow sequence is $a \rightarrow b \rightarrow c \rightarrow d$, and the flow behavior is as shown in Movie 3.

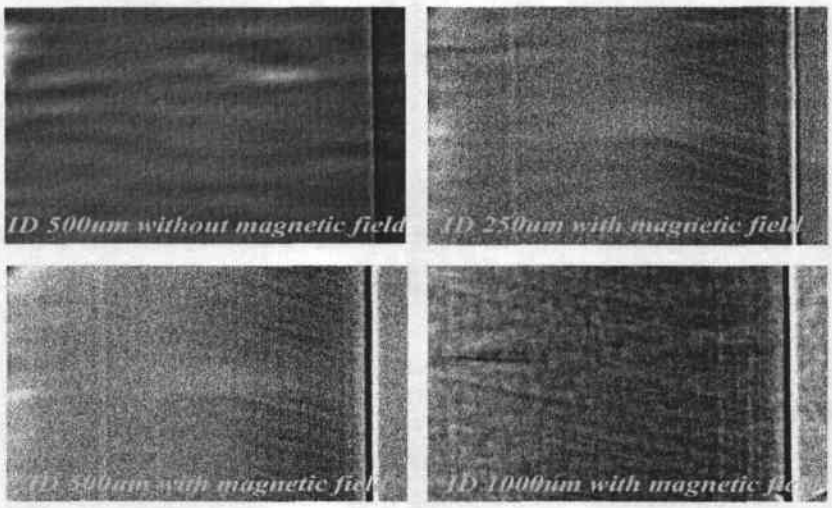

Figure 11. The figures show the motion of the magnetic nanoparticles in field by observing the movement of the aggregated nanoparticles. Detail of the flow is shown in

Movie 4.

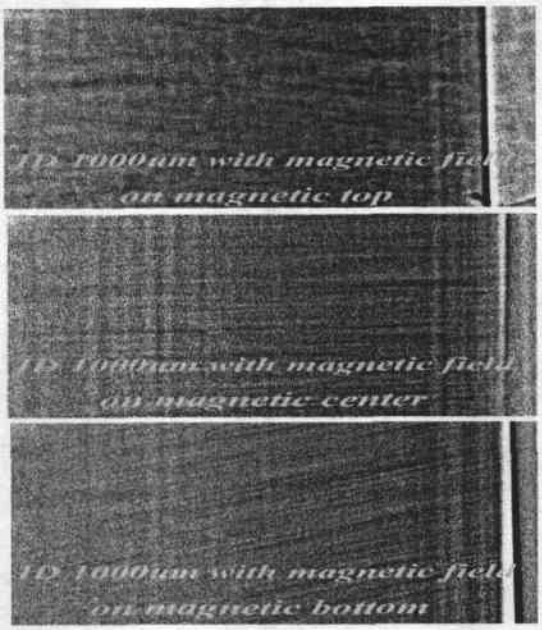

Figure 12. The motion of the magnetic fluid at different regions shows different characteristics due to the differences in field profiles. The behaviors are clearly shown in Movie (5), (6), (7).

Figure 12 shows, at a steady flow system, the shape and the flow pattern of the aggregated nanoparticles vary with the magnetic field lines. Based on these systematic observations, it is apparent that we can not detect the nanoparticles if they are uniformly dispersed in the fluid. We need to have some external contrast enhancers, such as the presence of air-bubble or the external magnetic field, to observe successfully the flow of the magnetic fluid. Thus, one approach to get better images of the fluid flow is to apply the magnetic field before turning on the Wriggle pump. Under this circumstance those particles near the tube wall, i.e., those much closer to the magnet, are flowing with a very small, or even steady speed. While those near the center of the tube flow with the pattern following the magnetic field lines. These effects were seen clearly in video (Movie.8).

III. Observations of magnetic fluid with different Fe_3O_4 concentration and in a set of magnets

There are two separate results in this part of experiment. First observation is concerning the effect of magnetic field, which generated by a single magnet, on the behavior of nanoparticles under different conditions such as concentration of nanoparticles; the second part is the effect under several magnets connect in series.

For the first part of the experiment we use four different samples with different Fe_3O_4 concentrations, and observe their behavior under different conditions as list in Table I. For the second part of the experiment we used the magnetic fluid that has 10 wt% Fe_3O_4 nanoparticles and observed its flow in a set of magnets connect in series. The experimental setup is the same as shown in Figure 8, and Table 1 lists the parameters we used in this experiment.

Table 1: Parameters set for the experiments

	Fe_3O_4 content (wt%)	Distance from wall (mm)	Flow speed (rpm)	Magnet arrangement	Remark
Test 1	10、8	2	0.1	One Piece	
Test 2	8、5、2	2	1.0	One Piece	
Test 3	10	6→1	0.1	One Piece	Moving step is 1mm
Test 4	10	4→1	3.0	One Piece	Moving step is 1mm
Test 5	2	6→12	3.0	One Piece	Moving step is 2mm
Test 6	10	6	5→7→10 →13	One Piece	
Test 7	10	6	7	Two in series	
Test 8	10	4	7	Two in series	

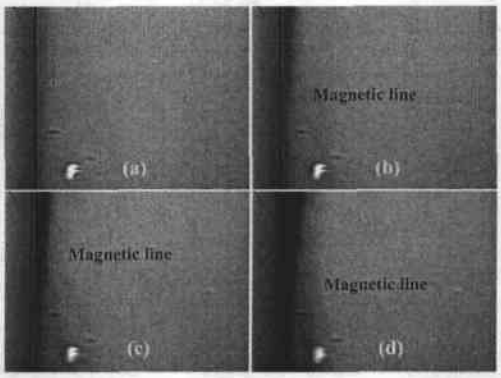

Figure 13. The movie (Movie 9) shows the flow pattern of the 10 wt% magnetic fluid under the influence of magnetic field with test 1 condition. The nanoparticles aggregate along the tube wall, which is seen as the darker region in the graph.

Based on our previous experiences, we observed a clear fine magnetic force line along the wall of the microfluid tube that contains 10 wt.% Fe_3O_4 under the influence of a single piece magnet which locates about 6 mm away. In the current experiment

we extend the observing time and used the testing condition 1 as listed in Table I. Figure 13 shows the observed motion of the magnetic fluid. Then we gradually reduced the concentration of the magnetic nanoparticle which under the same experimental condition and the result shown in figure 14 is for the sample with 8 wt% concentration.

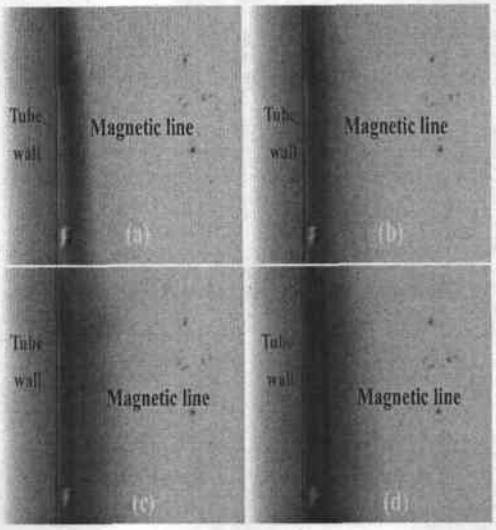

Figure 14. The movie (Movie 10) shows the magnetic flux lines of the 8 wt% magnetic fluid under the influence of magnetic field with test 1 condition.

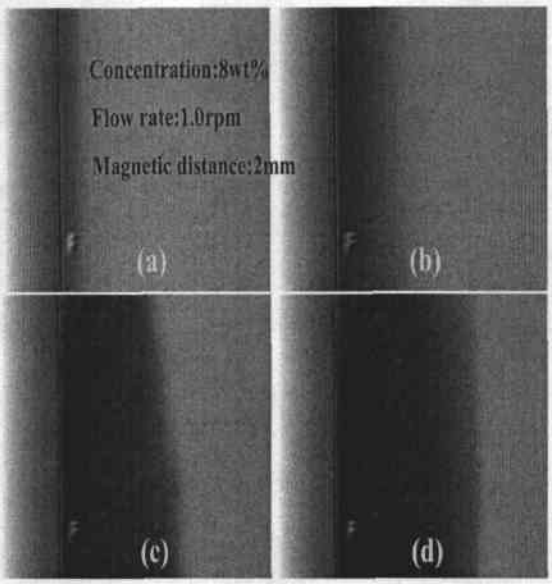

Figure 15. The movie (Movie 11) shows the flow pattern of the 8 wt% magnetic fluid under the influence of magnetic field with test 2 condition.

Experiment test 2 was to test the difference of the microfluid motion of different nanoparticle concentrations, but under exactly the same flow speed and the distance between magnet and the tube. The observations are shown in figures 15 to 17. The motion of the magnetic field lines for 8 Wt% sample is clearly observed, while it is not that obvious in the 5wt% and 2 wt% samples. At these lower concentrations we no

longer saw the uniform motion of the field lines, instead we saw the formation of some spherical objects, which are believe to be the accumulation of nanoparticle.

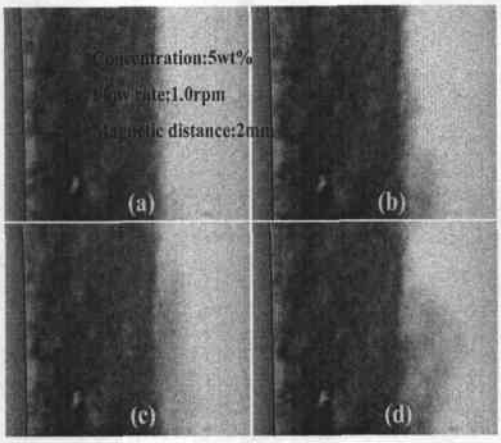

Figure 16. The movie (Movie 12) shows the flow pattern of the 5 wt% magnetic fluid under the influence of magnetic field with test 2 condition.

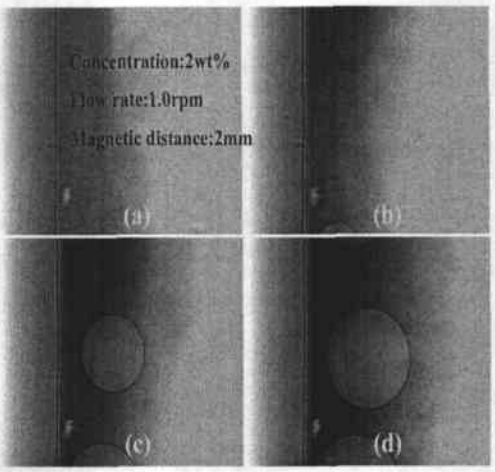

Figure 17. The movie (Movie 13) shows the flow pattern of the 2 wt% magnetic fluid under the influence of magnetic field with test 2 condition.

Furthermore, for the purpose of finding out the best observation parameters, we also tested the effects of the distance between magnet position and tube, and the flow speed. In this case, we used test conditions 3-5 in Table I and two different samples with 10 wt% and 2 wt% concentrations. Figure 18 is the outcome of test 3. The magnetic field lines increases as the magnet moves closer to the tube. Subsequently we increased the flow speed to 3 rpm and the results were not much changed as shown in figure 19. However, when we changed the sample to the 2 wt% one and under the same condition as in test 4, the results of test 5 are very much different. As shown in figure 20, we no longer saw the motion of the field lines, consistent with those observed in low concentration samples. What we observed were the formation of clusters and a thin layer of nanoparticles attached to the tube wall. Test 6 was designed to observe the effects of fluid flow speeds. It is clear that when the flow speed is higher than 10 rpm it greatly affected the attachment of the nanoparticles to

the tube wall, such as at 13 rpm, we could no longer see the thin nanoparticle layer along the wall, as shown in figure 21.

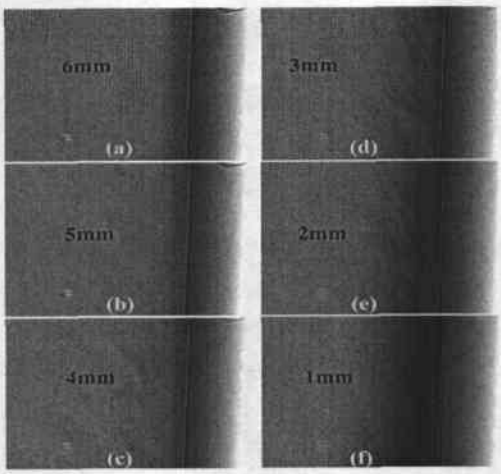

Figure 18. The fluid flow observed under test condition 3, which varies the separation between the magnet to the tube from 6 mm to 1 mm. The flow pattern can be seen in Movie 14.

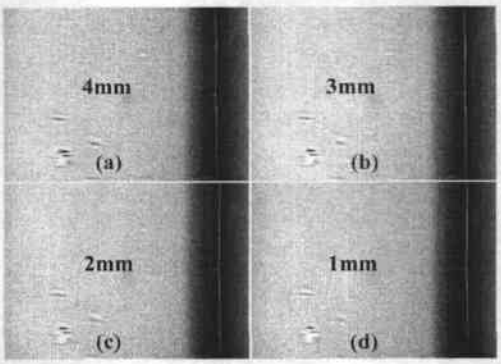

Figure 19. The fluid flow observed under test condition 4, which varies the separation between the magnet to the tube from 4 mm to 1 mm. The flow pattern can be seen in Movie 15.

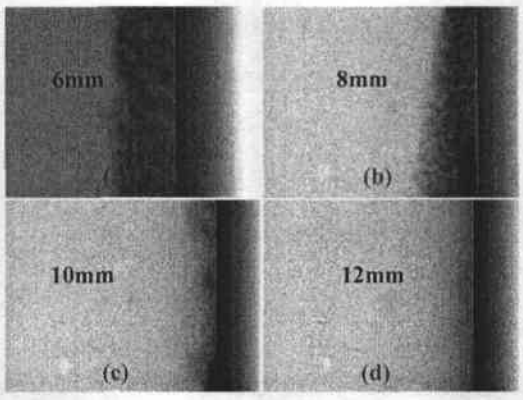

Figure 20. The fluid flow observed under test condition 5. The flow pattern can be seen in Movie 16.

The last part of the experiments, tests 7 and 8, were to observe the effects of two magnets connected in series on the magnetic fluid flow. As shown in figure 21, we

observed that the nanoparticles form a straight line along the wall at the region between the two magnets.

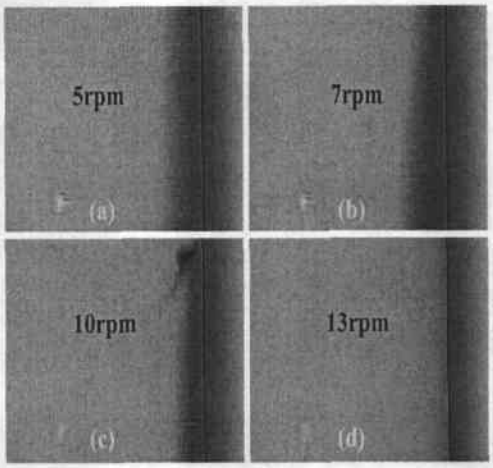

Figure 21. The fluid flow observed under test condition 6, which fixes the distance between the magnet to the tube (6 mm) but varies the flow speed with 5, 7, 10, 13 rpm, respectively.

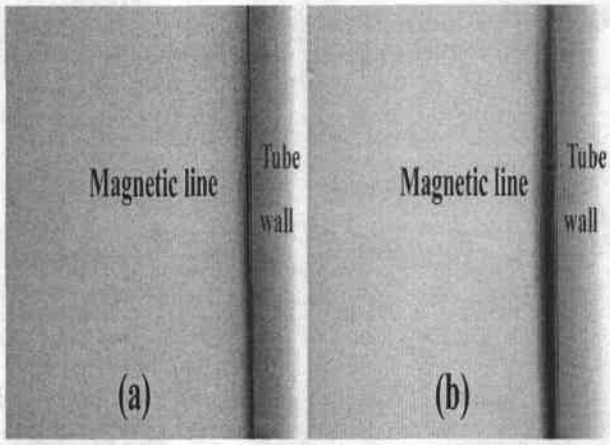

Figure 22. At flow speed of 7 rpm (Test 7 and 8) the image of the magnetic fluid flows between the magnets which are in series.

IV. Observations of magnetic fluid in magnets with different configurations

This set of experiments aims to study the properties of nanoparticles subjected to a magnetic field under two different magnetic field configurations: 1) with attractive poles in series and with the channel adjacent to the magnets 2) with opposing poles and the channels placed in the field center. We experiment with two methods of configuring the magnet: 1) with attractive poles in series and with the channel adjacent to the magnets 2) with opposing poles and the channels placed in the field center. For Method 1 we experimented with situations involving two and three magnets as shown in Figs 23 and 24. For Method 1 with two magnets, we fixed the distance between the channel and magnets at 6 mm and allowed the magnetic fluid to flow at 3, 7, 10, and 15 rpm. The channel diameter is 1000 um. These are listed as Test 1, 2, 3 in the table below as we also varied the fluid Fe_3O_4 concentration. For three magnets, we use a 10 wt% concentration fluid flowing at 3 rpm (Test 4). Finally,

we also experimented with the magnet configuration Method 2, listed in the table as Test 5 and shown as Fig 25.

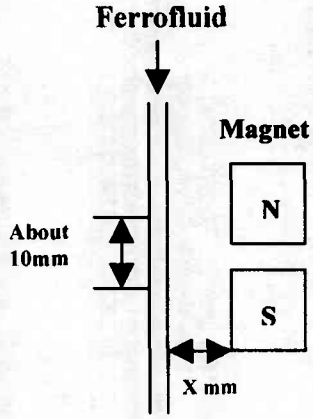

Figure 23. Schematic of the set-up with two magnets in series.

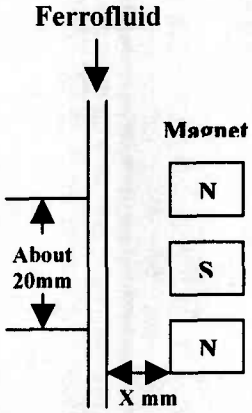

Figure 24. Schematic of the set-up with three magnets in series.

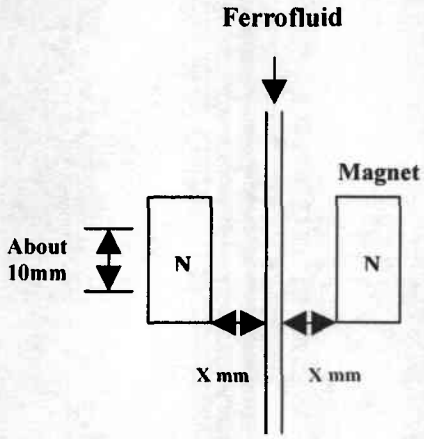

Figure 25. Schematic of the set-up with two magnets in parallel.

Table II. Parameters used in this set of experiment

	Fe_3O_4 content (wt%)	Distance from Tube (mm)	Flow Speed (rpm)	Magnet arrangement	Tube size (um)
Test 1	5	6	3、7、10、15	In series	1000
Test 2	10	6	3、7、10、15	In series	1000
Test 3	20	6	3、7、10、15	In series	1000
Test 4	10	0	3	In series	1000
Test 5	10	0	3、10	In parallel	500

Fig 26 shows the results of a 5 wt% fluid with varying flow speeds under the influence of the magnetic field. At low flow speeds, the field lines are thin, long strands, while at high flow speeds the field lines are broken. Increasing the Fe_3O_4 concentration to 10 wt%, we observe that for speeds below 10 rpm, the field lines maintain their thin shape, but at speeds higher than 10 rpm the lines are also broken, though near the channel edges some line shapes are visible, as shown in Fig 27. When the concentration is increased to 20 wt%, the field lines become much thicker and shorter, and the nanoparticle fluid flow is less affected by a change in flow speed. As in Fig 28, we see that less particles are stuck to the edge due to the magnetic field attraction as the flow speed is increased. Comparing Test 1 to 3, we conclude that for the same flow speeds, higher Fe_3O_4 concentration fluids have thicker and clearer field lines. In particular, for same flow speeds, 10 wt% concentration has the most uniform and clear field lines.

Figure 26: Test 1, the variation of field lines in the magnetic fluid with 5wt% Fe_3O_4 under fixed magnetic field but different flow speeds.

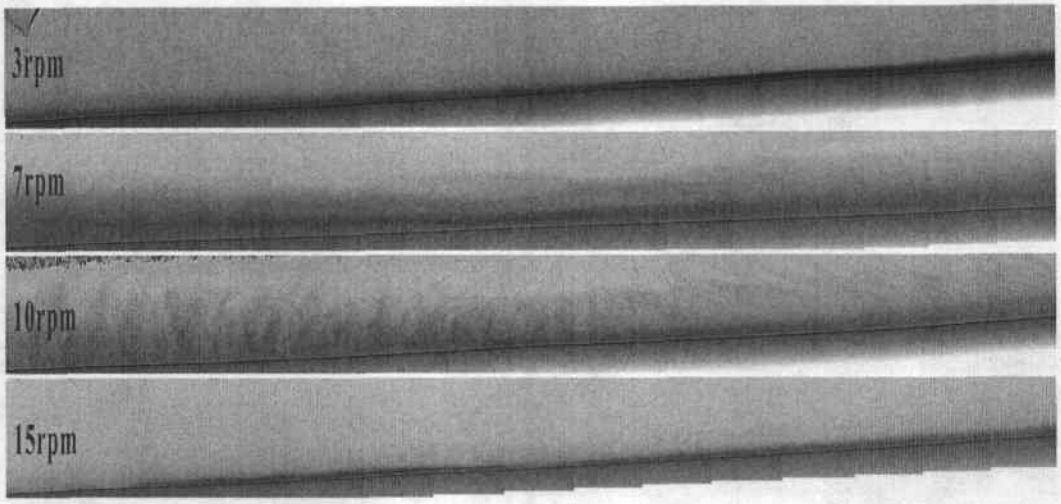

Figure 27: Test 2, the variation of field lines in the magnetic fluid with 10wt% Fe_3O_4 under fixed magnetic field but different flow speeds.

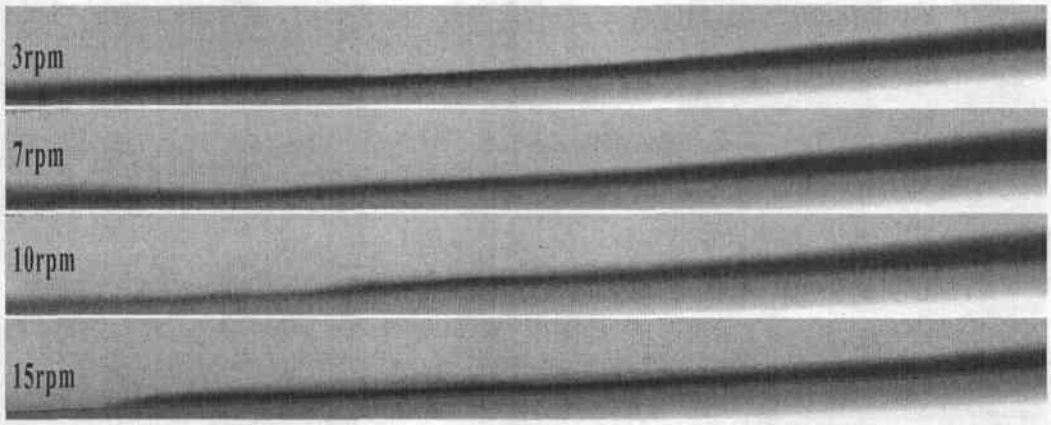

Figure 28: Test 3, the variation of field lines in the magnetic fluid with 20wt% Fe_3O_4 under fixed magnetic field but different flow speeds.

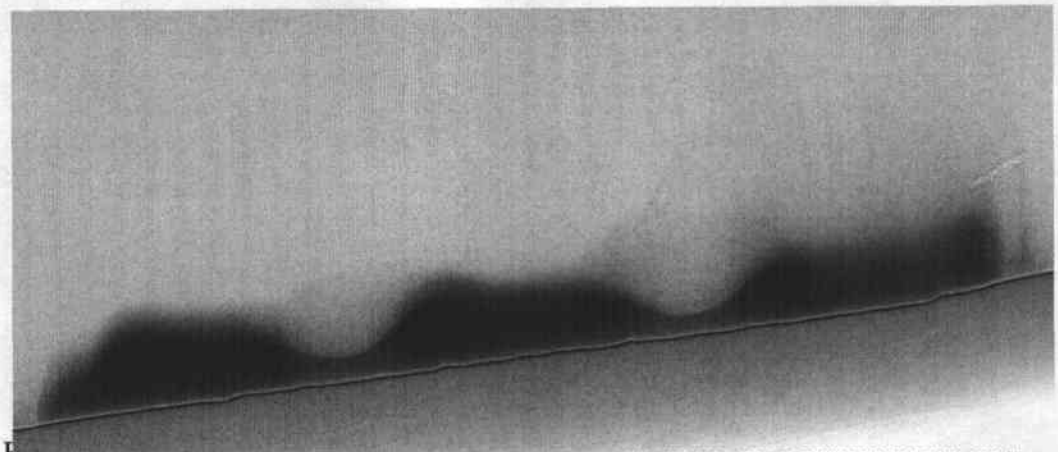

under the influence of three magnets set in series.

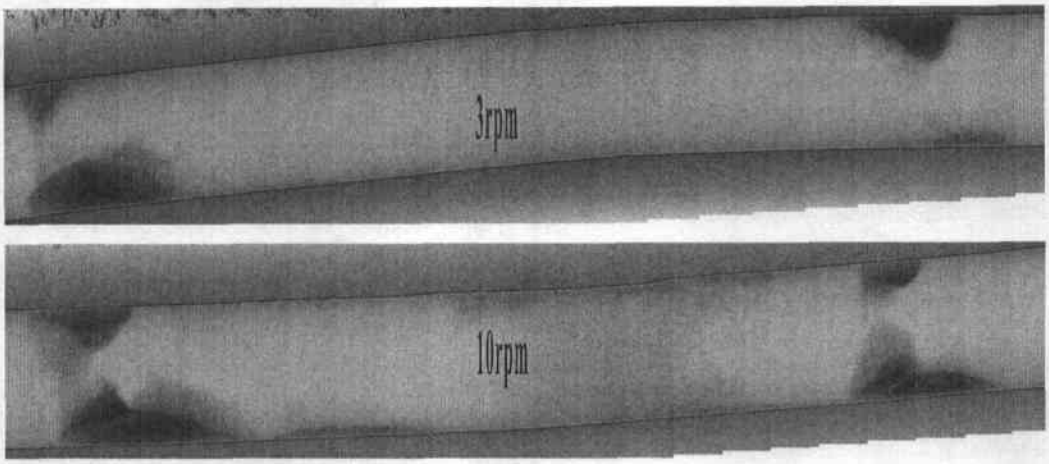

Figure 30. Test 5, the variation of field lines in the magnetic fluid with 10wt% Fe_3O_4 under magnets set in parallel but different flow speeds.

Fig 29 shows the results for Test 4. The magnetic field lines are thin and uniformly distributed along the channel. For Test 5 (Fig 30), we see the formation of a puddle of nanoparticles in the center of the magnetic field. This puddle largely maintains its shape regardless of the particle flow speed and is only affected by a change in field strength.

V. Summary

We have carried out extensive studies of the magnetic fluid flow with various Fe_3O_4 concentrations. The Fe_3O_4 particles synthesized have diameters of 90-100 nm. From the experiment we can conclude that the nanoparticle fluid behaviour can be tuned by controlled parameters. In particular, we have overcome the issue of aggregation of particles as the particles clearly form separate chains when flowing through the channel under the influence of a magnetic field. The magnetic field also works, similar to the introduction of air-bubble to the fluid, as a contrast enhancer to improve the X-ray microscopy image. Since the nanoparticles exhibit super-paramagnetic chacracteristic, their magnetism disappears as soon as the

magnetic field is removed. Thus, the use of the magnetic field is a very effective mean to achieve our objectives of using the microscopic radiology for imaging magnetic fluid in microchannel.

The obvious next step is to improve on Fe_3O_4 particle diameter control with the goal of growing particles with diameter ~50 nm, and to increase the fluid concentrations, so that the magnetic behaviour can be more clearly observed and the fluid purity is higher. In conclusion, we have magnetically tunable nanoparticles in fluid, and the next step is to decrease particle diameter and increase fluid purity.

The experimental results presented here provide us fruitful information for a more advanced study in order to improve the functionality of ink-jet printer head. the images of the internal bubble formation with the external formation of the sprays We are also very optimistic that with this initial results, we can study mechanism of nano-particle flow in micro-scaled fluidic channels, which may eventually lead to the better understanding of the mechanism of drug delivery. By the completion of this first study, we are ready to start a more complete investigation of a genuine microfluidic flow system that can be under control in order to achieve the ultimate goal of the creation of complex, highly integrated, microscale total analysis systems.

Acknowledgments

This work is not possible without the support from the Far-East Army Research Office in Tokyo. We like to thank particularly, Dr. Sean H.Y. Yu and Dr. Brett Pokines for their encouragement and support. We also want to thank Prof. J.H. Je of Pohang Univeristy of Science and Technology for his help and support in using the Synchrotron facility at Pohang.

References

1. C. J. Sun, G. M. Chow, J. P. Wang, E. W. Woo, D. Y. Noh, J. H. Je, Y. K. Hwu, Nucl. Instrum. Meth. **B199**, 156(2003).

2. W. L Tsai, Y. Hwu, C. H. Chen, L. W. Chang, J. H. He, H. M. Lin and G. Margaritondo, Nucl. Instrum. Meth. **B199**, 457(2003).

3. W. L Tsai, P.C. Hsu, Y. Hwu, J. H. Je, Y. Ping, H. O. Moser, A. Groso and G. Margaritondo, Nucl. Instrum. Meth. **B199**, 436(2003).

4. W. L Tsai, P. C. Hsu, Y. Hwu, C. H. Chen, L. W. Chang, J. H. He, A. Groso and G. Margaritondo, Nucl. Instrum. Meth. **B199**, 451(2003).

5. W. L Tsai, P. C. Hsu, Y. Hwu, C. H. Chen, L. W. Chang, J. H. He, A. Groso and G. Margaritondo, Nucl. Instrum. Meth. **B199**, 451(2003).

6. Jong Ryun. Kim, H.S. Kang, Ho Jun Lee, Jung Ho Je, S. K. Jeong, W. L. Tsai, P. C. Hsu, and Y. Hwu, Nucl. Instrum. Meth. **B199**, 441(2003).

7. Ho June Lee, Jung Ho Je, Y. Hwu and W.L. Tsai, Nucl. Instrum. Meth. **B 199,** 342(2003).